Evaluating the Effects of Electron Kappa Distributions on Collisionless Shock Dynamics in the Solar Wind

Leo A. Skaer[1], Colby C. Haggerty[1], Jason M. TenBarge[2], Lynn B. Wilson III[3]

[1] University of Hawai‘i at Mānoa Institute for Astronomy
[2] Department of Astrophysical Sciences, Princeton University
[3] NASA Goddard Space Flight Center, Heliophysics Science Division

UNIVERSITY of HAWAI'I® MĀNOA

Background

The effectively collisionless nature of astrophysical plasmas has proven a significant challenge to understanding how shocks disseminate flow energy into thermal energy within a given system. Without interparticle interactions providing an effective means of energy transfer, it is theorized that instabilities and waves generated by the shock will scatter particles and increase entropy of the system. Instabilities capable of causing this effective collisionality include electron cyclotron drift (ECDI), ion acoustic wave (IAW), modified two-stream (MSTI), Buneman, and lower-hybrid drift (LHDI), though the former three instabilities are considered more likely candidates than the latter two due based on observational, theoretical and simulation evidence (Wilson et al., 2021; Gary and Omidi 1987; Matsukiyo and Scholer, 2006; Krall and Liewer, 1971; Buneman, 1958)

Observation and Simulation Discrepancies

The majority of heliospheric shocks are aligned with the shock normal quasi-perpendicular to the magnetic field, and are supercritical with particle reflection providing an additional source of energy dissipation (Balogh and Treumann, 2013). Observations of the solar wind in the Earth's bow shock have revealed a number of differences from plasma simulations initialized with Maxwellian electron VDFs. One notable difference is the lack of large-amplitude, high-frequency electrostatic waves in simulations when compared to satellite data. As simulated IAWs and the ECDI are both strongly affected by the initialized velocity distribution of ions and electrons, modern kinetic simulations that assume isotropic Maxwellian electron VDFs are largely unable to generate the aforementioned electrostatic features observed consistently *in situ* (Wilson et al., 2022).

Particle Velocity Distributions

Direct measurements of electrons in the solar wind reveal 3 primary populations; core, halo and strahl (Borovsky et al., 2021). Core electron velocity distributions are bi-self-similar (of which Maxwellian VDFs are a subset), while strahl and halo electrons are better approximated with a kappa function (visually similar to a Maxwellian with extended power-law tails.) The solar wind velocity is supersonic to ion thermal sound speeds but subsonic to electron thermal sound speeds, thus ion VDFs can be sufficiently described by a Maxwellian whereas this approximation oversimplifies the existence of distinct electron populations, their associated VDFs, and the impacts these VDFs on shock dynamics (Wilson et al., 2021).

PIC Code: Tristan-MP

Particle in cell (PIC) codes provide a computationally efficient means of solving the Vlasov-Maxwell equations across a large parameter space. Tristan-MP, a three-dimensional relativistic PIC code, features dynamic memory allocation, current filtering and other novel methods to improve overall efficiency and reduce unwanted simulation instabilities and noise that PIC codes are prone to. Tristan-MP discretizes electric and magnetic fields across a 2D grid, calculating the motion of particles with the Lorentz force equation and subsequent changes to electric and magnetic fields at each grid point, ensuring second-order accuracy in both space and time evolution of the system (Hakobyan and Spitovsky, 2020).

Simulations

Three initial simulations were generated with different electron VDF inputs. Based on observational data, a kappa index value of 4 was chosen to simulate a realistic solar wind electron VDF. A strongly Maxwellian simulation with a kappa index of 20 serves as a point of comparison to more conventional plasma shock simulations. A third simulation with a kappa index of 3, considered a strong kappa distribution, was also included to investigate what effects overestimating the kappa distribution may have on instability generation. Each simulation has an Alfvénic Mach number of 7, quasi-perpendicular magnetic field angle of 70°, ion-electron mass ratio of 400, and sigma value of 0.01. After preliminary analysis and comparison of the three simulations, a higher-cadence simulation for $\kappa=4$ data was created to investigate specific features in greater detail.

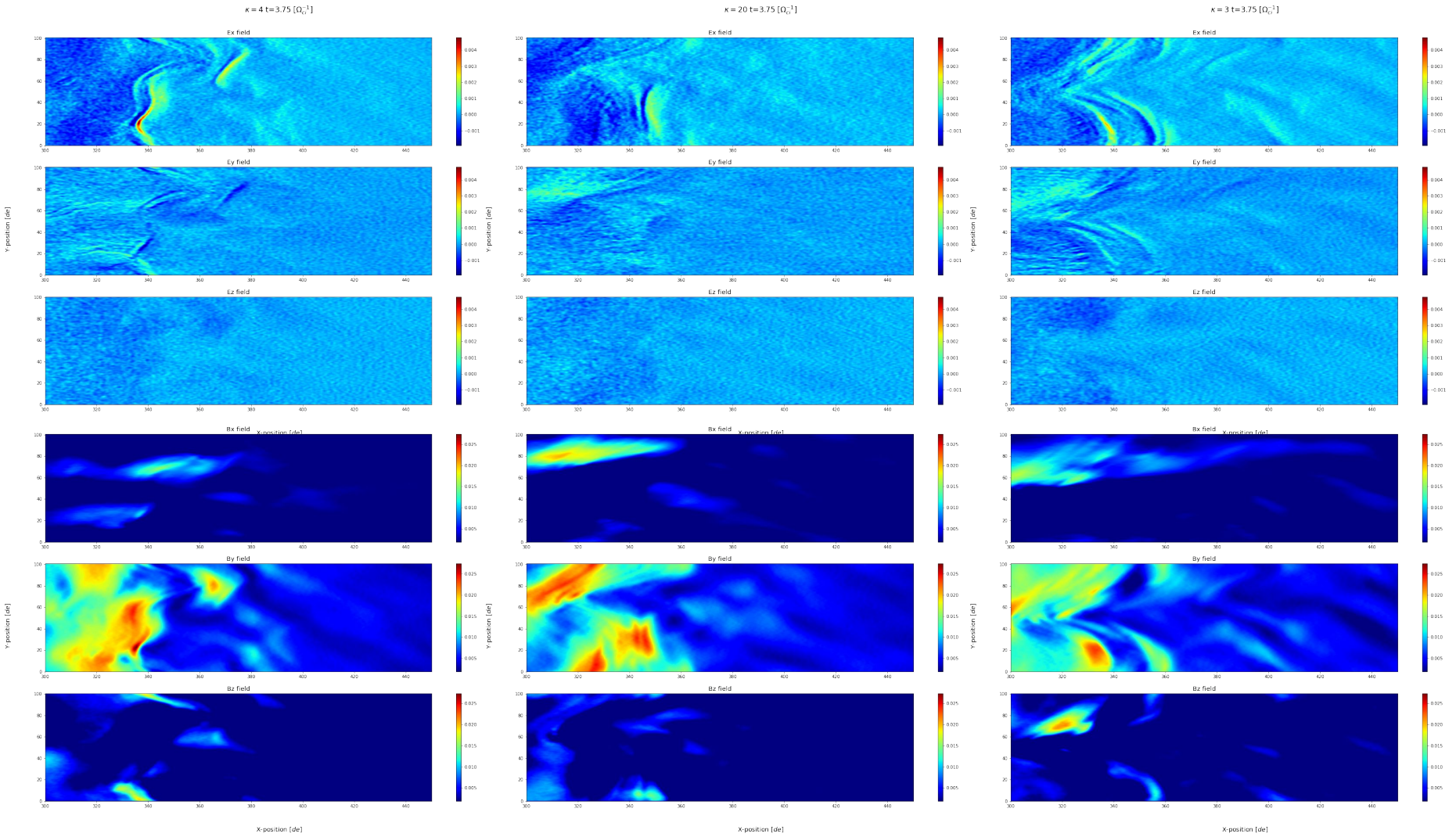
κ = 4 t=3.75 [Ω_ci^-1]
κ = 20 t=3.75 [Ω_ci^-1]
κ = 3 t=3.75 [Ω_ci^-1]
Ex field
Ey field
Ez field
Bx field
By field
Bz field
Y-position [de]
X-position [de]

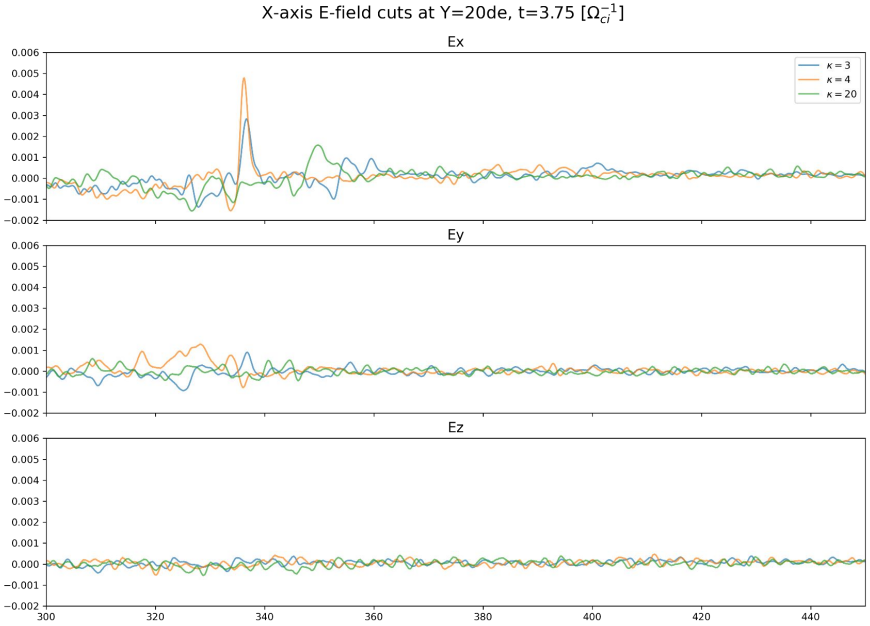
X-axis E-field cuts at Y=20de, t=3.75 [Ω_{ci}^{-1}]
Ex
Ey
Ez
$\kappa = 3$
$\kappa = 4$
$\kappa = 20$

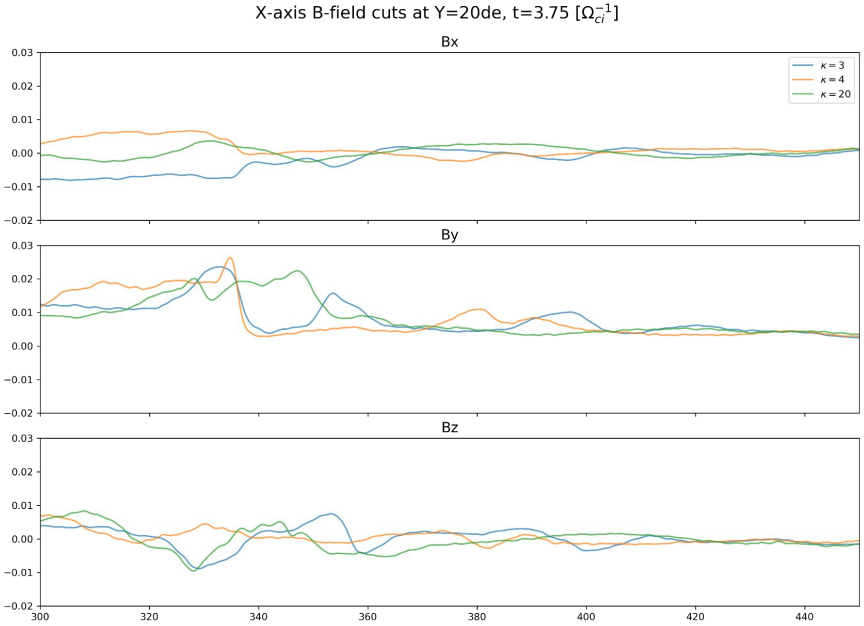
X-axis B-field cuts at Y=20de, t=3.75 [Ω_{ci}^{-1}]
Bx
By
Bz
$\kappa = 3$
$\kappa = 4$
$\kappa = 20$

Initial Simulation Observations

The grid space of each output was normalized to the electron inertial length (d_e) of the simulated shock, and the time domain was normalized to the shock inverse ion cyclotron frequency (Ω_{ci}^{-1}). Upon visual inspection of the electric field of each simulation, strong features were observed in the κ=4 simulation. Neither the κ=3 nor κ=20 simulations contained features of comparable magnitude. This discrepancy was also present in the magnetic fields of each simulation, though to a lesser degree. The peak of the κ=4 electric field fluctuations occurred at 3.75 Ω_{ci}^{-1}, and the high-cadence simulation was initialized around this time to explore the properties of this feature and potentially connect it with a progenitor instability.

High-Cadence Simulation

Using the timescale of the initial κ=4 simulation, the high-cadence simulation began at approximately 3.438 Ω_{ci}^{-1} and ran until approximately 4.687 Ω_{ci}^{-1}. There were 999 output files generated compared to the 13 of the first three simulations. The simulation was divided into three time segments and electric field peaks were recorded during each of these increments. The locations of these peaks were then used as test points to plot each feature's time domain evolution, along with taking x-direction cuts at the y-location of the peak to estimate physical wavelength. Additionally, hodograms were created for each peak as polarization can provide further constraints on possible progenitor instabilities.

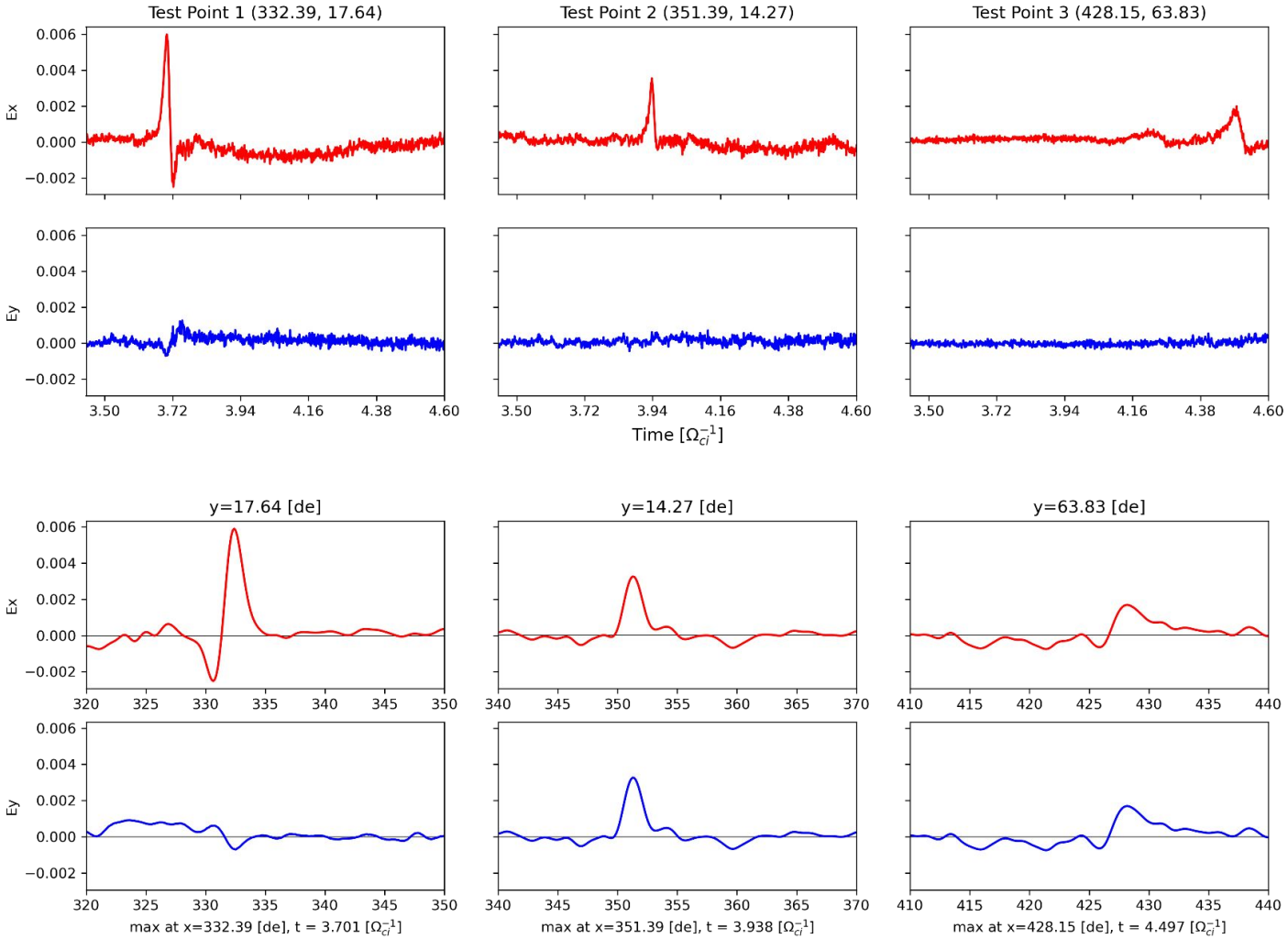
Test Point 1 (332.39, 17.64)
Test Point 2 (351.39, 14.27)
Test Point 3 (428.15, 63.83)
Ex
Ey
0.006
0.004
0.002
0.000
−0.002
3.50
3.72
3.94
4.16
4.38
4.60
Time [Ω_{ci}^{-1}]
y=17.64 [de]
y=14.27 [de]
y=63.83 [de]
320
325
330
335
340
345
350
340
345
350
355
360
365
370
410
415
420
425
430
435
440
max at x=332.39 [de], t = 3.701 [Ω_{ci}^{-1}]
max at x=351.39 [de], t = 3.938 [Ω_{ci}^{-1}]
max at x=428.15 [de], t = 4.497 [Ω_{ci}^{-1}]

Time & Space Measurements

In the time domain the waveforms captured at each test point appear as isolated pulses. The test point 1 wave features both a trough and peak, while the waves at points 2 and 3 do not. Electrostatic solitary waves (ESWs), which are frequently observed in astrophysical plasmas, can be generated by various instabilities including the MTSI and LHDI and appear as isolated pulses with frequencies ~10^1 ms and wavelengths greater than Debye length scales (Matsukiyo and Scholer, 2006; Wilson et al.,2021). ECDI-generated waves appear as asymmetric sine waves with frequencies of order 10^2-10^4 Hz and normalized wave number less than 1 on d_e length scales. The appearance of the test point 1 wave may be indicative of a strong ESW and lower-amplitude ECDI wave, which is strengthened by its wavelength of approximately 10 d_e (corresponding to a normalized k of < 1) (Wilson et al.,2021).

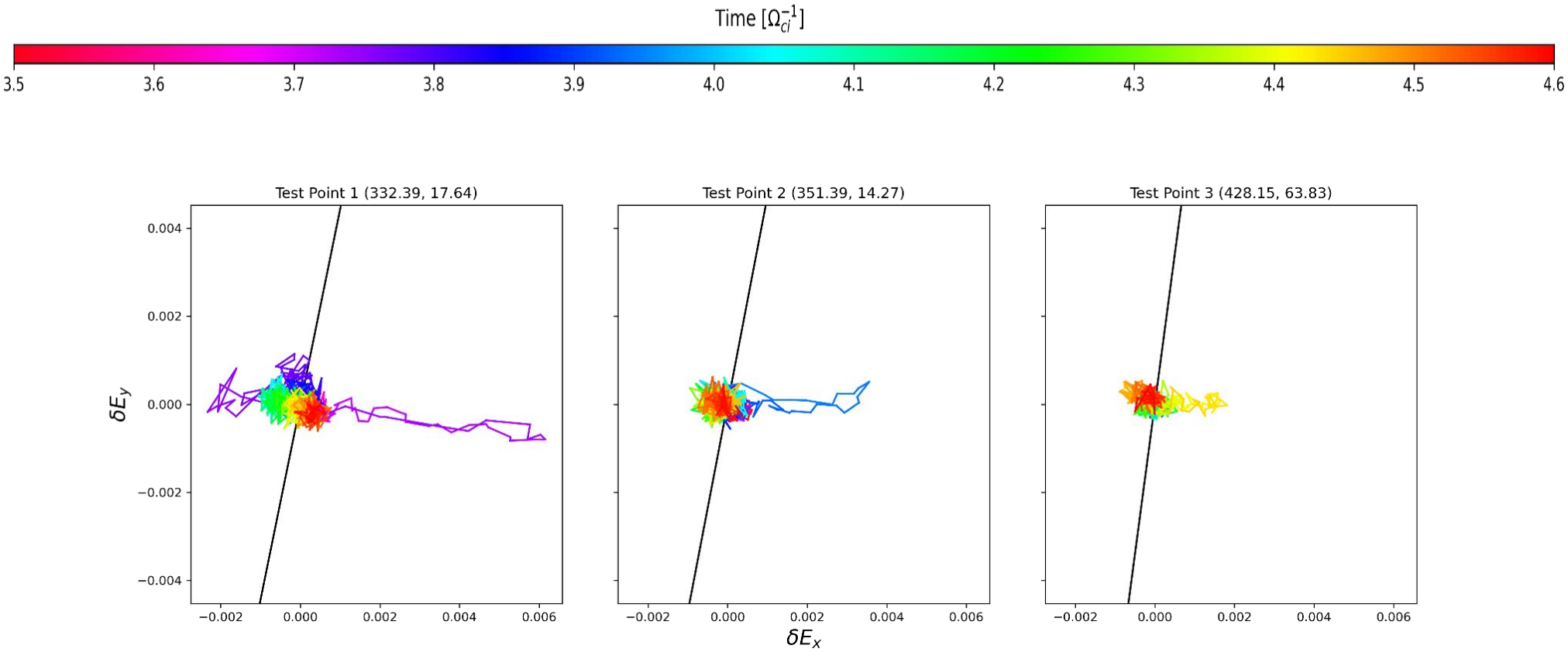
Time [Ω_{ci}^{-1}]
3.5
3.6
3.7
3.8
3.9
4.0
4.1
4.2
4.3
4.4
4.5
4.6
Test Point 1 (332.39, 17.64)
Test Point 2 (351.39, 14.27)
Test Point 3 (428.15, 63.83)
δE_y
δE_x
0.004
0.002
0.000
−0.002
−0.004
−0.002
0.000
0.002
0.004
0.006

Hodograms

All three peaks appear linearly polarized nearly perpendicular to the quasi-static magnetic field (B_0) with the strongest polarization features occurring at times corresponding to the respective electric field peaks. Points 2 and 3 are visually unipolar while point 1 displays asymmetric bipolarity. The magnitude of polarization corresponds to the amplitude of the wave in time and space, while the direction of polarization reflects the measured electric field strength in the time domain. The ECDI is characterized by a “teardrop” shaped polarity oblique to B_0, while ESWs can appear unipolar when perpendicular to B_0. As with the time and space measurements, the hodograms visually suggest the presence of strong ESWs and potentially smaller ECDI-driven waves.

Conclusions

Preliminary simulations have demonstrated that PIC code simulations of astrophysical plasma initialized with realistic kappa VDFs are capable of producing large-amplitude electrostatic waves not observed in Maxwellian simulations, nor simulations initialized with stronger and less realistic kappa electron VDFs. Higher-cadence exploration of the properties of these waves shows promise for connecting these waves to instabilities known to be capable of creating effective collisionality in astrophysical plasmas.

Further Research

More quantitative analysis of electrostatic wave features is required to conclusively determine the progenitor instabilities. Fourier analysis will allow constituent wave modes to be determined with greater accuracy, which can be compared with known frequency ranges of potential progenitors. This analysis can also be performed for more high-cadence simulations, as only one timestep was chosen for this stage of the project but the initial simulations contain multiple points and features worth exploring in greater detail. Furthermore, though the MTSI is less directly impacted by non-Maxwellian electron VDFs it would be worth investigating potential differences as it remains an important secondary instability in shocks, particularly in supercritical quasi-perpendicular shocks.